1. INTRODUCTION

The present thesis is concerned with the dynamic aspects of damage in composite laminates. Damage in composite laminates generally takes the form of micro cracking in the matrix material, delamination of plies, fiber-matrix debonding and fiber fracture. The damage will lessen the stiffness of the material and alter, among other things, the dynamic properties of the material. The formation of damage will also release mechanical waves, which can be measured. Analysis of the measured signals is an aid in attempts to understand and quantify the damage mechanisms.

1.1 The Use of Composite Materials

Polymer based composite materials are characterized by their high stiffness and strength-to-weight ratio, and owing to their inherent anisotropy it is possible to optimize load bearing capacity on the material level. The main drawback is that they are relatively expensive to manufacture, especially continuous, or advanced, fiber composites. Therefore, continuous fiber composites have so far found their application in areas where weight is of great concern and cost is not. Advanced composites are commonly used in sporting equipment (where perhaps cost is a concern!) such as rackets, hockey sticks and golf clubs. Another example is sailing boats, both for recreation and competition. The prime examples are, however, aerospace applications. It is of course very important to save weight on objects launched into space, and the increased manufacturing cost is of less concern since many of the objects are made in very small numbers - if not unique - so in these cases design is much more expensive than manufacture.

A classical area for light and stiff construction is airplane design. Prior to World War II, wood was the most commonly used structural material. The stronger engines developed prior to and during the war, however, increased the forces on the airplanes and called for more complex fuselage and wing designs, so the material choice shifted to the newly developed aluminum alloys. This has been, and still is, the most important material in the airplane industry, but the amount of composite materials in airplane structures is increasing. In high performance military airplanes such as JAS 39 Gripen, Lockheed F-22 and Boeing B-2 composite materials account for more than 20% of the structural weight. Composites have also found their way to civilian airplanes, in the Boeing 777 9% of the structural weight is composites. Composites are, however, still mainly used in non-critical parts such as wing panels and one reason, apart from cost, for this is that the behavior of aluminum is much better understood than that of composites.

2. COMPOSITE LAMINATES

A composite material can roughly be defined as a material with two (or more) distinct macroscopical phases. Often the morphology of the composite is such that one material, the matrix, surrounds the other. The surrounded material can for example have spherical, fibrous or disc shaped form, and when it comes to structural materials, fiber composites are most common. This has its origin in the fact that many materials can be manufactured with a much higher tensile

strength in fibrous than in bulk form. Glass for example has a relatively high stiffness-to-weight ratio but is virtually worthless as a structural material. The reason is, as everybody knows, that glass is very brittle. One small imperfection within a body of glass can trigger instable crack growth, and for glass in bulk form this is critical, whereas the fracture of one fiber in a bundle is not. The advantages of surrounding the fibers with a matrix material are that the matrix keeps the fibers in place, distributes load among them and protects them from external damage. In the case of structural fiber composites, polymers, such as epoxy, are commonly used as matrix materials.

2.1 Laminates

A widely used geometry for continuous fiber composites is the laminate. Laminates are made of plies, in which all fibers often have the same direction. The fibers are usually much stronger and stiffer than the matrix so a ply is stiffer and stronger in the fiber direction - it is anisotropic. A laminate, such as the one shown in Figure 1, usually contains plies with different fiber directions even if the load is primarily in one direction. The reason is that a laminate with fibers in only one direction would be very weak in the direction transverse to the fibers, and small transverse loads due to uneven lateral contraction, for example, could trigger fracture of such a laminate.

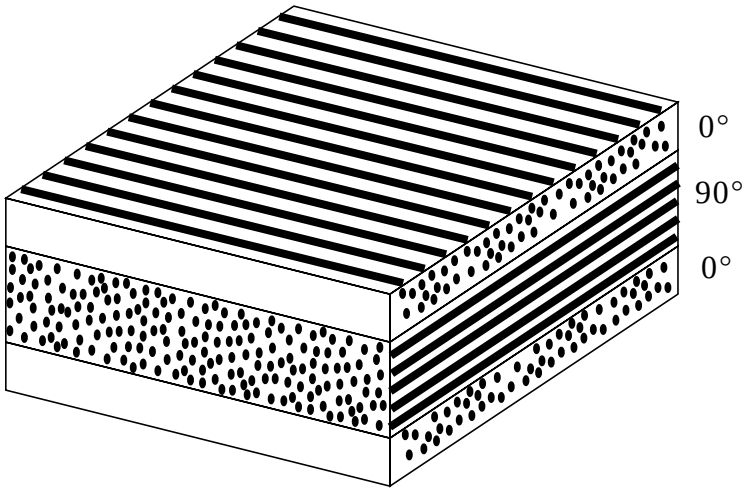

Figure 1 *A* $[0/90_2/0]$ *or* $[0/90]_S$ *laminate.*

Laminate geometry is described by the direction of the fibers in its plies. The laminate in Figure 1 would, for example be labeled $[0/90_2/0]$. The direction of the fibers in the outer plies are in this case chosen as the reference direction, the $0°$-direction, and the middle ply, which is twice as thick, has its fibers directed $90°$ to the reference direction. Another way to label the laminate is $[0/90]_S$ where 'S' stands for symmetric. The anisotropic nature of the laminate opens a possibility of design and optimization on the material level, so the distinction between material and component or structure becomes less clear than it is for design with metals.

The static elastic response on the global level of an undamaged laminate is well understood and can be predicted using well established models. In order to use laminated composites effectively and safely there is, however, also a need for understanding and prediction of damage in laminates.

2.2 Damage in Composite Laminates

For safe and efficient use of composite laminates in structures it is important to understand inelastic material behavior. In metals, plasticity and creep are examples of such inelastic behavior. In polymer based fiber composites, an important type of inelastic behavior has its origin in the micro damage, that appears as the load on the material increases. In polymer based continuous fiber composites the development of damage often starts with matrix cracking transverse to the principal load direction, see Figure 2. This is followed by fiber fracture and delamination between plies, possibly aided by stress concentration at the tips of the existing matrix cracks. This scenario has been seen in many experiments [4,7].

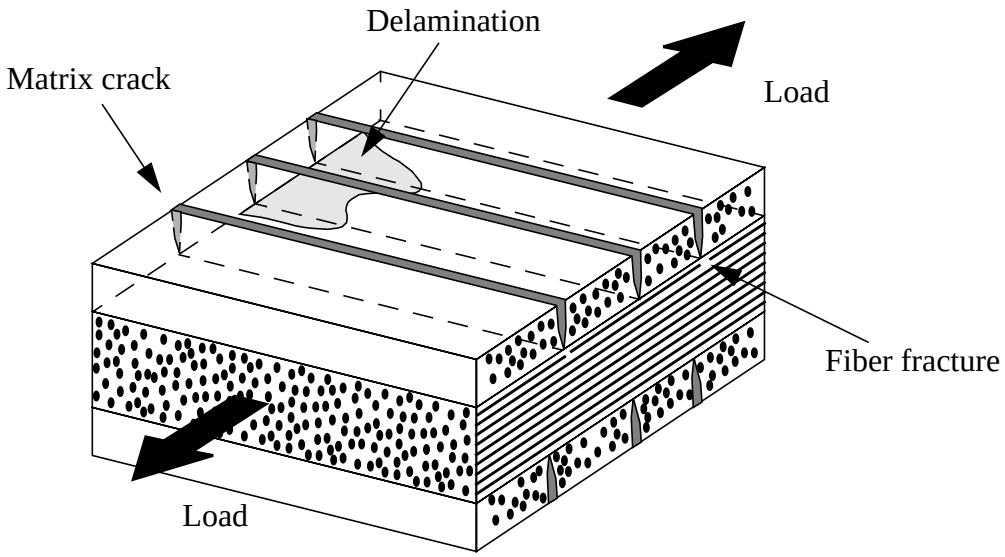

Figure 2 *Common damage types in composite laminates.*

Mathematical models for predicting the behavior of damaged composite materials are of great value, and a lot of work has been done in this area. Ideally the model should have the character of a constitutive relation for the material. That is, component size and geometry, and preferably laminate lay-up (order of ply stacking), should not enter the material model directly. Real constitutive relations, like Hookes' law for linear elastic materials, have the advantage that material properties can be measured on one geometry and transferred to another. For example, the elastic deformation and stress in a pressure vessel of steel can be calculated using constitutive parameters (Young's modulus and Poisson's ratio) obtained from a uniaxial test of the steel.

The constitutive description of damaged composite materials have two basic parts. The first, and usually easiest part, is the behavior of the composite at a given damage state. The second part describes the development of damage during loading. The approaches to the problem can very roughly be divided into two groups - continuum damage mechanics and micromechanics.

The continuum damage mechanics approach is based solely on measurements of the global, or overall, response of the material, and the goal is to generalize the measurements done for particular geometries and loads to a constitutive relation. If plasticity is regarded as a damage state in metals, then von Mises' model for plasticity would be an example of successful application of continuum damage mechanics.

The other approach, micromechanics, attempts to model the damage mechanisms on the microlevel (in the case of plasticity, this would be models of dislocation movement) and predict the global behavior. Micromechanics is often, at least in principle, successful in predicting the response for a given damage state. Development of damage is more complicated, because information about the material parameters and geometry on the microlevel is hard to obtain. The main reason is the small length scales involved. The plies in composite laminates are typically 0.125 mm thick and the diameter of the fibers is about 1/100 mm. Modeling of matrix crack formation and growth in laminates, in particular, requires knowledge regarding the position of the crack, the stress state the crack is experiencing, crack tip velocity and so on. Part of this information can be obtained after the formation of the crack by x-ray, edge replica *et c.*, but there is also a need to follow the formation of the crack in time. This can be done by recording and analyzing the stress waves released in the laminate by a growing crack, so called acoustic emission.

3. ACOUSTIC EMISSION

The object of acoustic emission is to gain knowledge about an event by recording the mechanical waves it releases. Seismology is an old branch of acoustic emission. Responses, in form of motion of the earth's crust, are recorded in different parts of the world and these recordings can be used to tell where the event took place, how big it was and whether it was an earthquake or something else. The analysis of earthquakes has in fact spurred a lot of the research regarding wave propagation in solids. For example, Rayleigh and Love waves were discovered in attempts to explain observations from earthquakes [6]. Rayleigh waves travel on the surface of a solid (not unlike waves on water) and Love waves exist in the border between an elastic layer and its substrate.

The response due to an earthquake usually lasts for several seconds and therefore the recording systems used do not have to be very fast. The formation of damage in composite laminates, for example matrix cracks, on the other hand, is a very fast event, which is measured in tens of microseconds. In order to resolve the time signal very fast recording systems, including modern computer technology, have to be used.

A typical acoustic emission experimental set-up for composite laminates is schematically

shown in Figure 3. In this case acoustic emission in a uniaxial test specimen is measured. The uniaxial specimens used are typically 2 cm wide and 20 cm long. Damage generates a wave which propagates through the specimen, and the transducer responds to this wave. The electrical signal from the transducer is then amplified and filtered before it enters an analog-digital converter where the continuous signal is translated to a sequence of samples. The sampling rate of the A/D converter should be at least 10 MHz. After sampling the signal is filtered and amplified again before it is stored.

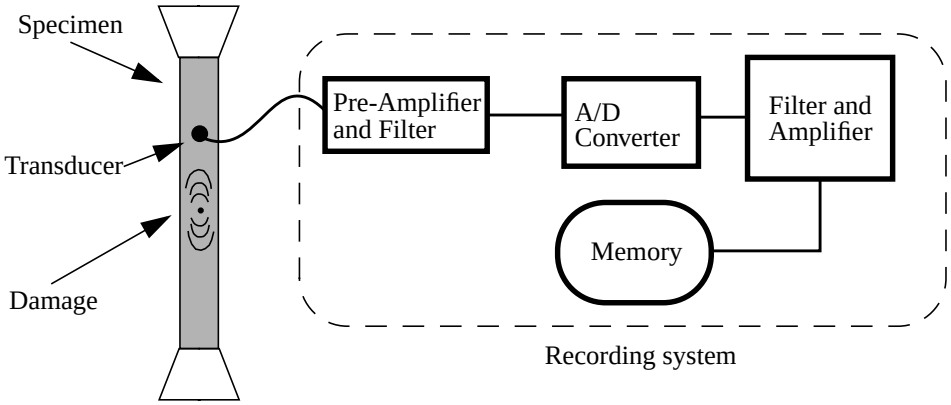

Figure 3 *A typical acoustic emission experimental set-up.*

Acoustic emission analysis is an inverse problem in the sense that a signal is recorded and its cause is wanted. One way to do the analysis is by a direct approach, where the distortion of the signal from a postulated event is modeled. The analysis can be performed by dividing the acoustic emission chain into four parts. Damage (or source) modeling, wave propagation from source to transducer, transducer response to surface movements and response of the recording system. In frequency domain this can be described by three transfer functions as shown in Figure 4.

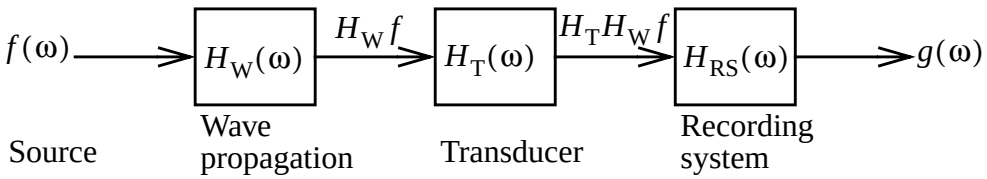

Figure 4 *The acoustic emission chain in frequency domain.*

The postulated event produces a signal, $f(\omega)$, which is distorted as the wave travels through the specimen, $H_W(\omega)$. The resulting signal is also changed as it passes from the specimen through the transducer, $H_T(\omega)$, and in to the recording system, $H_{RS}(\omega)$, before it is stored as the signal $g(\omega)$. The distortion due to the transducer and transducer characteristics are briefly discussed below.

3.1 Transducers

The transducer is critical because it provides input to the recording system, and no subsequent signal conditioning can make up for bad transducer behavior. Therefore transducers have been the object of a substantial amount of research and development, see for example [5]. Figure 5 shows a schematic diagram of a transducer. The active part in a transducer is the piezoelectric element, which generates an electric potential when deformed. This element is usually made of a piezoelectric ceramic and is often circular in shape.

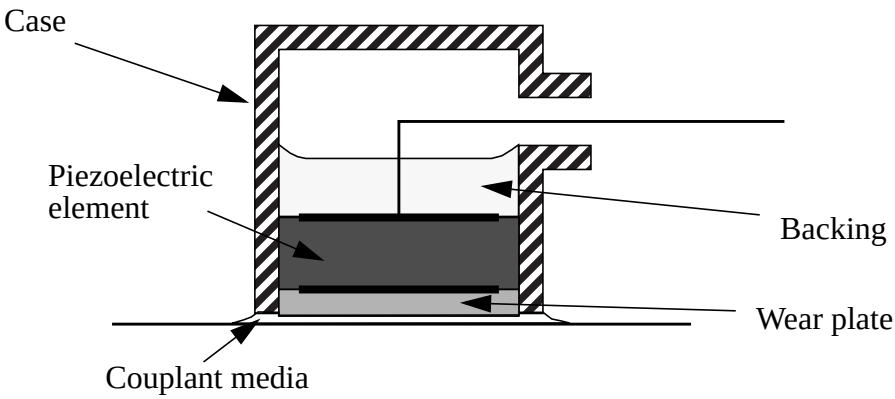

Figure 5 *A schematic diagram of a transducer.*

The element is protected by the wear plate, which is in contact with the surface under observation via a couplant media, such as grease. The object of the couplant media is to ensure an even contact between the wear plate and the surface. The case provides packaging for the transducer and makes handling easier. An important part of the transducer is the backing, which is often made of cured epoxy with a suspension of heavy particles such as tungsten. Its purpose is to allow waves to propagate away from the piezoelectric element with a minimum of reflection, and to provide damping in order to give the transducer a flatter frequency response. A flat frequency response is desired because it gives less distortion when the surface motion is translated to variation in voltage.

Figure 6 shows a simple mechanical model of the transducer. The spring constant, k, is mainly related to the size and shape of the piezoelectric element, the viscous damping, c, is governed by the backing, and the mass, m, is the effective inertia of the transducer system. The amplitude, $|u^*|$, of the frequency or impulse response of the system can be written as

$$|u^*| = \sqrt{\frac{\alpha^2\left(\frac{\omega}{\omega_n}\right)^2 + 1}{\left[\left(\frac{\omega}{\omega_n}\right)^2 - 1\right]^2 + \alpha^2\left(\frac{\omega}{\omega_n}\right)^2}},$$

where the natural frequency of the undamped system is $\omega_n = \sqrt{k/m}$, and the damping parameter is $\alpha = c/\sqrt{km}$.

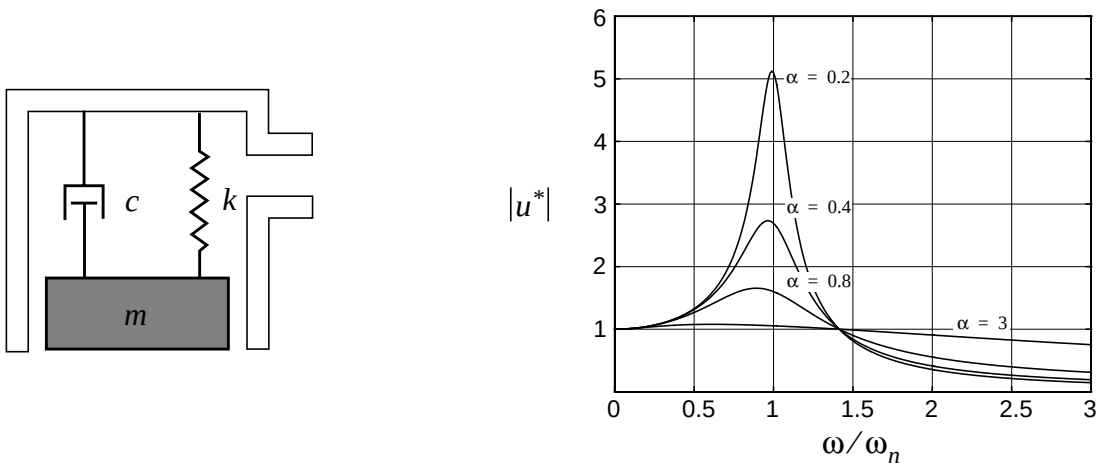

Figure 6 *A simple transducer model and its frequency response.*

The frequency response is shown for different values of α in Figure 6, and as can be seen high damping provides a flatter frequency response at the expense of sensitivity. The values of k and m can also be varied to provide a flat response in the frequency range of interest, but the physical dimensions of the transducer are strongly related to these parameters, and this limits the possible variation. Modern transducers (for example B1025 by Digital Wave Inc.) are of course much too complex for the model above and they have a fairly flat frequency response from 50 kHz to 1 MHz and are also very sensitive.

Typical transducers are 10 mm in diameter and this gives them limited wavelength resolution for waves which produce an uneven surface motion under the transducer, see Figure 7. A model of the phenomenon is found in [5]. Consider the interaction between a plane wave, $U(x,t)$, and a transducer with radius a. The average displacement under the transducer, $u(t)$, can be written as

$$u(t) = \frac{U_0}{a^2\pi}\int_{-a}^{a}\cos(kx-\omega t)\sqrt{a^2-x^2}\,dx,$$

where U_0, ω and k are the amplitude, circular frequency and wavenumber, respectively, of the incident plane wave. If it is assumed that the transducer response is proportional to $u(t)$, the output may be estimated from

$$u(t) = \frac{2J_1(ka)}{ka}U_0\cos(\omega t),$$

where J_1 is a Bessel function of the first kind. The sensitivity of the transducer depends in other words on the wavenumber or the wavelength. This is shown in the diagram in Figure 7.

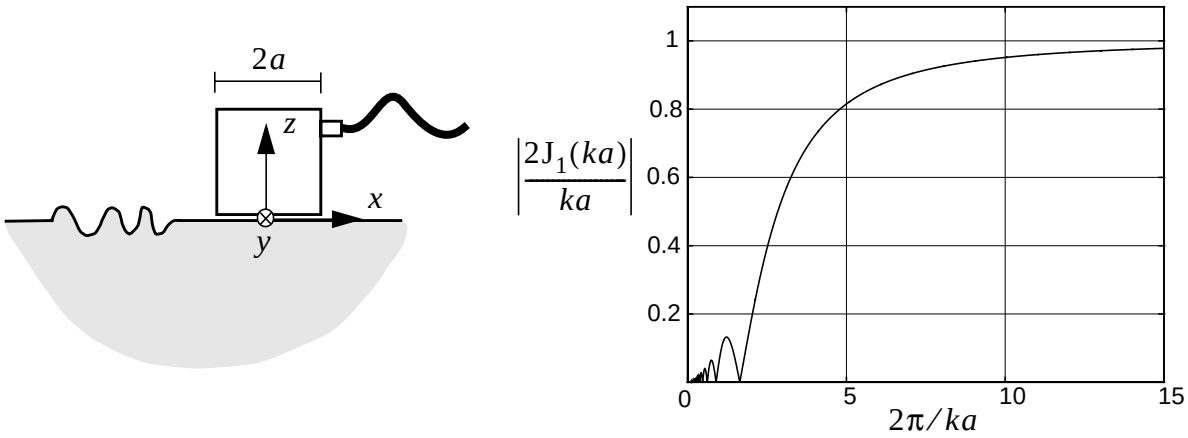

Figure 7 *Transducer wavelength resolution.*

The models above are, as discussed, very simple and at the best give qualitative information about transducer behavior. In practice the frequency response of the last two links in the acoustic emission chain (H_{T} and H_{RS}) shown in Figure 4 are found through calibration of the equipment. In the light of the discussion above regarding surface waves, it is important that this calibration is performed on the type of waves (surface or body waves) that will be measured.

The source and wave propagation are on the other hand possible and useful to model. Useful, because the frequency response, H_{W}, is very dependent not only on the geometry and lay-up of the specimen but also on the location of the source. To complicate things further, the damage development will alter the wave propagation characteristics of a laminate. This was studied in **paper 2**. Experimental determination of H_{W} is in other words a laboring task. The wave motion resulting from transverse matrix cracking and fiber fracture is modeled in the appended **papers 3** and **4** of this thesis.

4. WAVE PROPAGATION IN COMPOSITES AND WAVEGUIDES

Wave propagation in solids can often be modeled using linear strains and linear material behavior. The governing differential equations are linear, and a general wave displacement field can therefore be written as a superposition of harmonic waves with different wavelengths and frequencies. It may even be argued that the concepts of wavelength and frequency are intimately connected with linear wave motion.

The linear differential equations governing waves in a homogeneous isotropic infinite solid are

$$[(\lambda + \mu)\delta_{rs}\delta_{jl} + \mu\delta_{jr}\delta_{ls}]u_{r,ls} = \rho\ddot{u}_j, \tag{1}$$

where u_i and ρ are the displacement and density, respectively. The stiffness is expressed using Lame's constants λ and μ, and δ_{ij} is Kronecker's delta. Differentiation with respect to spatial coordinates and time are denoted by a comma and a dot, respectively. The usual summation convention is also used. Plane wave solutions for the above equation are considered, that is,

$$u_r(x_m, t) = Ad_r e^{i(kn_m x_m - \omega t)}, \tag{2}$$

where i is the imaginary unit, d_r and n_m are unit vectors, k is the wave number and ω the circular frequency. This results in the following relation

$$\{[(\lambda + \mu)n_r n_j + \mu\delta_{jr}]k^2 - \omega^2\rho\delta_{jr}\}d_r = 0, \tag{3}$$

which is a system of equations for the unknown components d_r. The condition for a non-trivial solution is that

$$\mathrm{Det}(\{[(\lambda + \mu)n_r n_j + \mu\delta_{jr}]k^2 - \omega^2\rho\delta_{jr}\}) = 0. \tag{4}$$

This is called the dispersion relation because it gives a relation between ω and k, that in general (but not here) has the effect that different frequencies travel at different velocities. The solutions d_r are called modes of wave propagation. In the present case the solutions can be found by rearranging equation (3)

$$k^2(\lambda + \mu)(n_r d_r)n_j + (\mu k^2 - \omega^2\rho)d_j = 0. \tag{5}$$

This vector equation has two solutions,

$$\omega = k\sqrt{\frac{\mu}{\rho}} \qquad \bar{n} \perp \bar{d} \tag{6}$$

or

$$\omega = k\sqrt{\frac{2\mu + \lambda}{\rho}} \qquad \bar{n} \parallel \bar{d}. \tag{7}$$

The waves described by equation (6) and (7) are called shear and dilatational waves. As mentioned earlier the relation between ω and k is in general non-linear. This means that the different frequency components in the superposed wave will travel at different velocities, because the velocity is given by

$$c_g = \frac{\partial \omega}{\partial k}. \tag{8}$$

The distance between the fast frequency components and the slower components will increase as the wave propagates, resulting in a *dispersion* of the wave, hence the term.

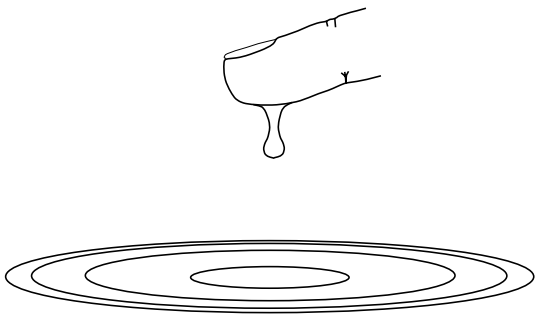

Figure 8 *Dispersion of water waves.*

Dispersion is an everyday phenomenon and there is even a saying relating to it - '... as rings on the water'. Ordinary water waves are dispersive! If a large pebble is thrown in to water a local disturbance is created. If water waves were non-dispersive one single ring would propagate outwards, but since velocity increases with wavelength, for these gravity controlled waves, the disturbance is dispersed, and a ring pattern is formed with the largest wavelengths at the outer edge. Smaller disturbances, such as rain drops, cause wave motion controlled by surface tension, and for those waves velocity decreases with wavelength. The ring pattern formed in this case have the shortest wavelength at the outer edge, see Figure 8.

In the analysis of wave motion from, for example acoustic emission, the infinite body solutions above are useful only if, the distance between the source and the receiver is smaller than the dimensions of the body and the wavelengths considered are much larger than inhomogeneties in the body. If this is not the case, reflections from outer boundaries and the interfaces between different components, such as fiber and matrix, become important. Reflections in solids are complicated by a phenomenon called mode conversion. An incident shear wave can for example result in reflected shear and dilatational waves, so keeping track of the resulting field after a large number of reflections is quite demanding. Nevertheless, circular symmetric wave propagation in homogeneous plates, which have two boundaries, have been studied in this way by Ceranoglu and Pao [3]. The maximum distance between source and receiver in that work was 6 plate thicknesses, which is too small in many situations. For some geometries it is possible to use another approach than keeping track of reflections. In the case of composites, for example, it is sometimes possible to analyze a unit or typical cell instead, and for plates or rods the cross section can be studied.

4.1 Composites

In the case of composites there are two basic approaches. One is to assume that the composite is periodic and analyze a periodic cell, and the other is to ‘smear out’ the inhomogeneties and calculate average, or effective, dispersion relations and displacement fields from a representative geometry. Considering fiber composites in particular, the different philosophies can be symbolized by Figure 9. The geometry pictured in Figure 9 relates to the averaging method called the generalized self-consistent scheme. This was used by Yang and Mal [8] to study wave propagation in composites (more references on average property methods can be found in the introduction to **paper 1**). The fiber, in that case, is embedded in the matrix material, which in turn is embedded in an effective medium with unknown properties. Given a certain circular frequency, ω, an effective or average wavenumber, $\|k\|$, is computed. The relation between ω and $\|k\|$ is in general non-linear.

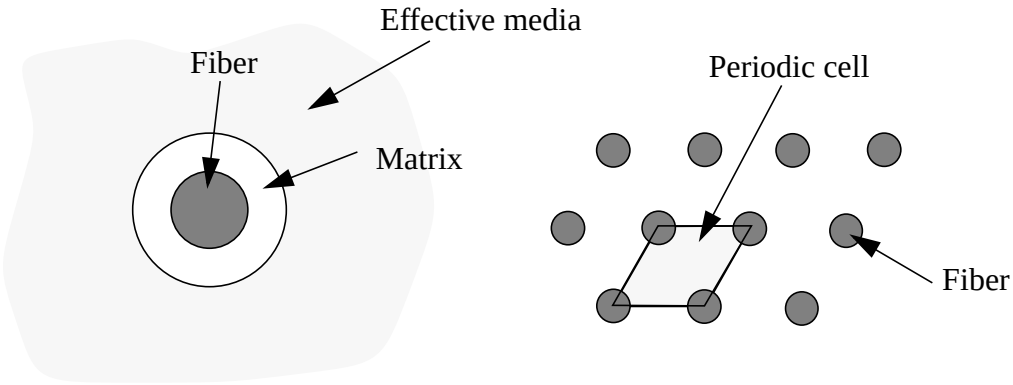

Figure 9 *The effective media and periodic cell approaches to composites.*

The effective wavenumber, $\|k\|$, can be real, complex or imaginary, where a real value corresponds to propagating waves and complex or imaginary values correspond to attenuated (or damped) waves.

The other approach is to approximate the geometry of the composite with a periodic one. Thanks to the translational symmetry, harmonic wave propagation in the composite can be studied by solving the equations of motion for a periodic cell subjected to boundary conditions which depend on the wavenumber (references on this approach are also found in **paper 1**). Although the boundary conditions are formulated using complex valued displacements and stresses it is possible to use standard finite element codes to solve the equations of motion. This is done by using one mesh for the real part and one for the imaginary part, and then couple the meshes with the boundary conditions. An eigenfrequency computation is performed, and the resulting eigenfrequencies give the dispersion relation. For a given wavenumber, several eigenfrequencies, or branches, with different displacement patterns exist (see Figures 6 and 7 in **paper 1**). The method is presented in **paper 1**. A shortcoming is that only propagating waves, *i.e.* waves with real valued wavenumbers, can be studied.

4.2 Waveguides

The behavior of 1- and 2- dimensional waveguides such as bars and plates can be examined by studying the cross section, which is perpendicular to the direction of wave propagation. For 1-dimensional waveguides the cross section is a surface and for 2-dimensional it is a line segment, see Figure 10. Exact solutions for isotropic homogeneous circular rods have been derived by Pochhammer and for homogeneous plates by Rayleigh and Lamb, see [6]. In both cases it is possible to find a series solution by postulating a displacement field in the form of an harmonic wave in the axial or in-plane directions. Fulfillment of the boundary conditions on the free surfaces give an homogeneous system of equations, with frequency and wavenumber as parameters, for the coefficients in the series. The dispersion relation is found by demanding a non-trivial solution, and the resulting coefficients determine the different mode forms.

Except for the special cases mentioned above, solutions for waveguides have to be found numerically or approximately. This can be done by assuming a cross section displacement field and deriving differential equations and boundary conditions with the help of Hamilton's principle.

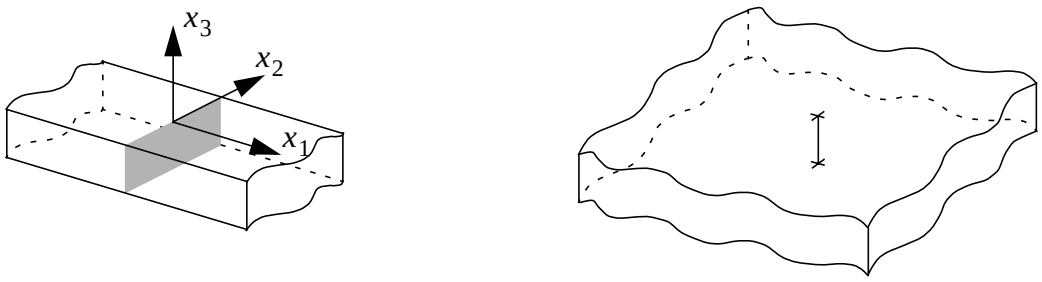

Figure 10 *Cross sections for 1- and 2- dimensional waveguides.*

For, example the simple displacement field

$$\begin{cases} u_3(x_i, t) = w(x_1, t) \\ u_1(x_i, t) = x_3 \psi(x_1, t) \end{cases}, \tag{9}$$

for the 1-dimensional waveguide in Figure 10 leads along with Hamilton's principle to Timoshenko's beam equations for bending. Note that the beam displacements w and ψ only depend on one coordinate and time. In **paper 3** a displacement field containing several beam displacements was used to study extensional and bending waves in laminated beams. An alternative to using fields for the whole cross section is to discretize it with finite elements. For the 1-dimensional case the nodal displacements will, like beam displacements, be functions of the axial coordinate and time. Aalami [1] was the first to use this approach for waveguides, and it was used in **paper 4** for laminated beams.

The differential equations for the beam or nodal displacements are in general coupled. Employing Fourier transforms in time and axial coordinate to these equations, or assuming harmonic wave propagation, leads, as for the exact solutions, to a system of equations for the displacements, in which the frequency and wavenumber (or, equivalently the transform variables) act as parameters. In the absence of volume forces the system of equations is homogeneous, and the dispersion relation is a result of requiring non-trivial solutions. For a given wave number, there will be several possible frequencies, or branches, one for each degree of freedom. The displacement solutions for each branch describes its displacement pattern. The complexity of these patterns increase with increasing frequency and wavenumber, so for a given wavenumber the branches with higher frequency will have more complex displacement patterns than those with lower frequency. Therefore an assumed displacement field will have a limited range of validity in frequency and wavenumber. Equation (9) for example describes only the lowest mode of bending for beams. The range of validity of one displacement field can be determined by comparing its dispersion relation to that due to a more sophisticated displacement field. This was done in **papers 2** and **3**, and to some extent in **paper 1**.

4.3 Transient Problems

The above mentioned solutions to the homogeneous problem can be used to express the transient wave field that results from transient nodal or generalized beam forces and time dependent end or boundary conditions. This can be done by subjecting the loads to the same transforms used to solve the homogeneous problem and then superposing the displacement solutions. The result is a formal solution in transform variables, and to get the time response this formal solution must be inverted.

In **papers 3** and **4** transverse matrix cracking and fiber fracture was translated to transient generalized beam forces and nodal forces, respectively. The translation was based on the work by Burridge and Knopoff [2], who have shown how displacement discontinuities, such as cracks, can be replaced by dynamically equivalent volume forces. The methods used to invert the formal solutions in **papers 3** and **4** are perhaps best illustrated through an example. The example will also, hopefully, shed some light on other issues discussed above such as dispersion.

4.4 Two Examples

Consider an infinite elastic rod loaded by the volume force

$$F(x,t) = F_0\delta(x)T(t), \tag{10}$$

where $\delta(x)$ is Dirac's delta function and the time dependence $T(t)$ is triangular in shape, see Figure 11. The motion in the rod will be calculated using two different differential equations. The

first is the regular wave equation for thin rods and the second is Love's rod equation.

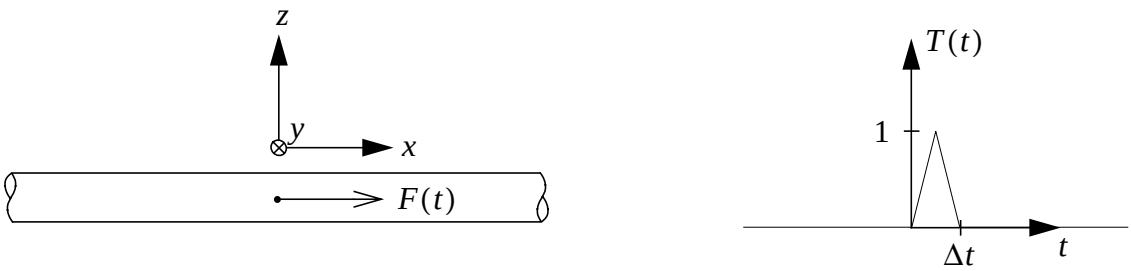

Figure 11 *A rod loaded by a time dependent volume force.*

The regular rod equation is

$$\frac{\partial^2 u_0}{\partial x^2} + \frac{F(x,t)}{E} = \frac{1}{c^2}\frac{\partial u_0}{\partial t^2}, \tag{11}$$

where E is Young's modulus of the rod and $c = \sqrt{E/\rho}$, where ρ is the density of the rod material. The volume force F is given by equation (10). The following Fourier transform pairs are introduced to solve the differential equation

$$\hat{g}(\xi,t) = \int_{-\infty}^{\infty} g(x,t)e^{-ix\xi}dx \quad , \quad g(x,t) = \frac{1}{2\pi}\int_{-\infty}^{\infty} \hat{g}(\xi,t)e^{ix\xi}d\xi \text{ and} \tag{12}$$

$$g^*(x,\omega) = \int_{-\infty}^{\infty} g(x,t)e^{i\omega t}dt \quad , \quad g(x,t) = \frac{1}{2\pi}\int_{-\infty}^{\infty} g^*(x,\omega)e^{-i\omega t}d\omega\,. \tag{13}$$

Transformation of equation (11) and rearrangement gives

$$\hat{u}_0^* = \frac{F_0 T^*}{E\left(\xi^2 - \frac{\omega^2}{c^2}\right)}, \tag{14}$$

which must be inverted to get the time response. In this case inversion is easily performed by the use of tables for example, but for the purpose of illustration the method used in **papers 3** and **4** will be used here. Also, the displacement velocity $\dot{u}_0$ will be calculated instead of u_0. Rewrite equation (14)

$$\hat{\dot{u}}_0^* = -i\frac{F_0 c T^*}{2E}\left(\frac{1}{\xi - \frac{\omega}{c}} - \frac{1}{\xi + \frac{\omega}{c}}\right), \tag{15}$$

where the relation $\dot{u}^* = -i\omega u^*$ has been used. Start by inverting with respect to ξ

$$\dot{u}_0^* = -i\frac{F_0 c T^*}{4\pi E}\int_{-\infty}^{\infty}\left(\frac{1}{\xi - \frac{\omega}{c}} - \frac{1}{\xi + \frac{\omega}{c}}\right)e^{ix\xi}d\xi . \tag{16}$$

For a given ω this integral can be evaluated by extending the real valued ξ to complex values. If the analysis is limited to $x > 0$ and a semi-circle in the upper half plane is added to the path of integration, the contour in Figure 12 results. With the use of residue calculus equation (16) may be expressed as

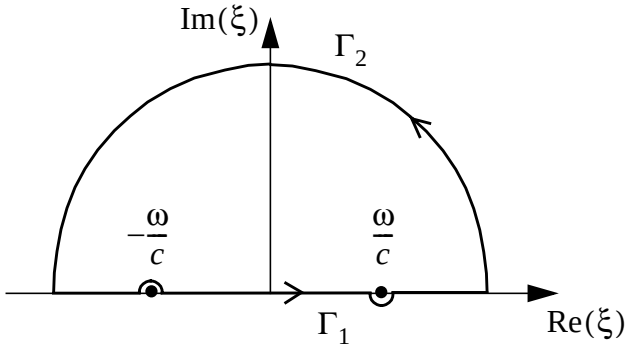

Figure 12 *Path of integration in the complex plane.*

$$\dot{u}_0^* = -i\frac{F_0 c T^*}{4\pi E}\left[2\pi i \mathrm{Res}(I_1) - \int_{\Gamma_2} I_1 d\Gamma_2\right], \tag{17}$$

where I_1 is the integrand in equation (16), and the first term is the sum of the of the residues of the poles inside $\Gamma_1 + \Gamma_2$. In this case the integrand has two poles, $\xi = \pm\omega/c$, on the real axis. These relations are the dispersion relations, because given a value of ω only two values of ξ are allowed. It is not self evident which poles should be included, but by adding a small damping term in equation (11) it can be shown that poles with $c_g = \partial\omega/\partial\xi > 0$ move upwards, in to the upper half plane, and vice-versa. From a physical point of view this is reasonable since $x > 0$ and waves with $c_g > 0$ move in the positive x-direction. Therefore, only the pole $\xi = \omega/c$ should be included, and the residue in equation (17) becomes

$$\mathrm{Res}(I_1) = e^{i\frac{\omega}{c}x} . \tag{18}$$

The second term in equation (17) will vanish. Let $R > |\omega/c|$ be the radius of the circle. For ξ on Γ_2 the factor in front of the exponential in I_1 then follows the relation

$$\left|\frac{2\omega/c}{R^2 e^{2i\theta} - \left(\frac{\omega}{c}\right)^2}\right| \le \frac{2|\omega/c|}{R^2 - \left(\frac{\omega}{c}\right)^2}, \tag{19}$$

which means that

$$\left|\int_{\Gamma_2} I_1 d\Gamma_2\right| \leq \frac{2|\omega/c|}{R^2-\left(\frac{\omega}{c}\right)^2}\left|\int_0^{\pi} e^{-Rx\sin\theta} R d\theta\right| \leq \frac{2|\omega/c|}{R^2-\left(\frac{\omega}{c}\right)^2}\frac{\pi}{x}, \tag{20}$$

where the last inequality follows from Jordan's inequality. The last expression in relation (20) will clearly vanish as R approaches infinity. Returning to equation (17) it is seen that

$$\dot{u}_0^* = \frac{F_0 c T^*}{2E} e^{i\omega\frac{x}{c}}, \tag{21}$$

which has the inverse transform

$$\dot{u}_0(x,t) = \frac{F_0 c}{2E} T\left(t-\frac{x}{c}\right). \tag{22}$$

The wave propagation analyzed above was non-dispersive, which is seen in equation (22). Taking lateral contraction into account by assuming the displacement field

$$\begin{cases} u(x,y,z,t) = u_0(x,t) \\ v(x,y,z,t) = -\nu y\dfrac{\partial u_0}{\partial x} \\ w(x,y,z,t) = -\nu z\dfrac{\partial u_0}{\partial x} \end{cases}, \tag{23}$$

where ν is Poisson's ratio, results in Love's rod equation,

$$\frac{\partial^2 u_0}{\partial x^2} + \nu^2 r^2 \frac{\partial^4 u_0}{c^2 \partial x^2 \partial t^2} + \frac{F(x,t)}{E} = \frac{1}{c^2}\frac{\partial^2 u_0}{\partial t^2}, \tag{24}$$

where r is the radius of gyration for the cross-section. Following the same scheme as above for $x>0$ gives,

$$\dot{u}_0^* = \frac{F_0 c T^*}{2E}\frac{1}{\sqrt{1-\nu^2 r^2\left(\frac{\omega}{c}\right)^2}} e^{i\omega\frac{x}{c}\sqrt{1-\nu^2 r^2\left(\frac{\omega}{c}\right)^2}}, \tag{25}$$

and the accompanying dispersion relation is given by

$$\xi = \frac{\omega}{c}\frac{1}{\sqrt{1-\nu^2 r^2\left(\frac{\omega}{c}\right)^2}}. \tag{26}$$

Equation (25) can be inverted by FFT if it is evaluated for a discrete set of values in ω (**paper 4**) or, for large values of x, by the stationary phase method (**paper 3**).

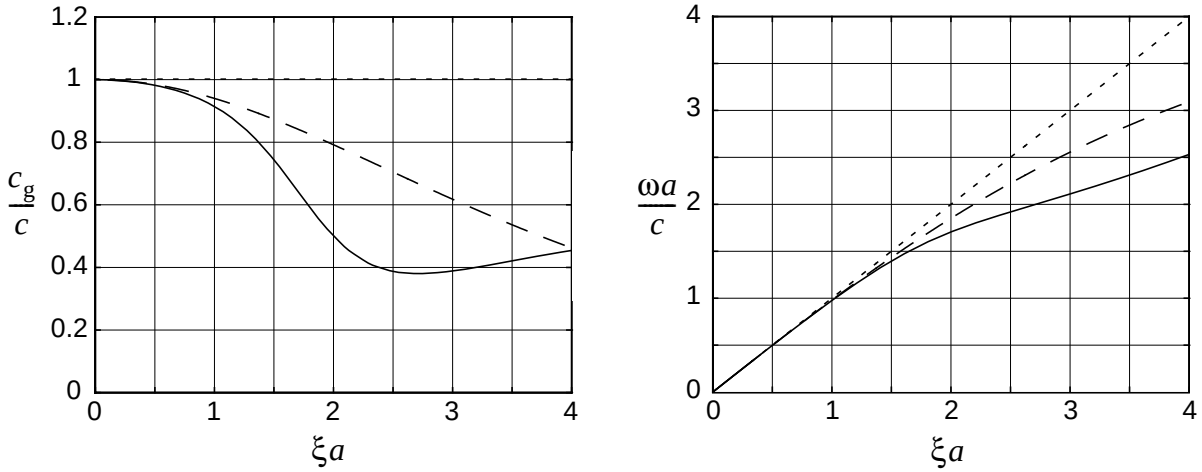

Figure 13 *Dispersion relations for non-dispersive rod equation (· - - - -), Love's rod equation (- - -) and exact (——)*

Figure 13 shows a comparison between the dispersion relations due to the ordinary wave equation (dashed), Love's rod equation (long dashed) and the exact result due to Pochhammer (solid) for a rod with circular cross-section and $\nu = 0.29$. Wave components with long wavelengths (small ξ) move faster than those with short wavelengths, as is seen in the left most diagram in Figure 13. It is also seen that Love's rod theory is valid only down to wavelengths of about $6a$, but it has the right qualitative behavior. Figure 14 shows the displacement velocity due to a volume force according to equation (10). The force's time dependence has triangular shape, as shown in Figure 11, with $\Delta t = 30a/c$. The response according to the ordinary rod equation does not change as the wave progresses because the wave propagation is non-dispersive. The response according to Love's equation, on the other hand, has been dispersed from its original triangular shape. The long wavelength components are found at the front, as is predicted from Figure 13, and the pulse is more spread in time and has lower maximum amplitude than the undispersed, or original, pulse (compare with water waves). This is typical for dispersive wave propagation.

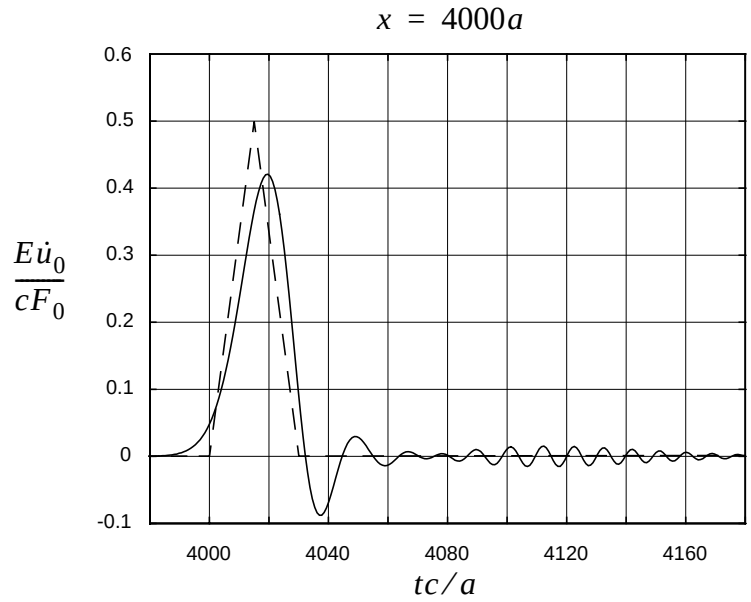

Figure 14 *Dispersion of triangular pulse. The response according to the ordinary rod equation (– – –) and according to Love's rod equation (——).*

5. SUMMARY OF APPENDED PAPERS

Paper 1 *The usage of standard finite element codes for computation of dispersion relations in materials with periodic microstructure.* Harmonic wave propagation in periodic structures, or composites, can be analyzed by studying a unit cell subjected to boundary conditions, which are formulated using complex valued displacement and stress fields. In the method presented, the complex valued displacement fields are split in to real and imaginary parts and one finite element mesh for each part is used. The identical meshes are coupled using the boundary conditions, and the wavenumber enters as a parameter in this coupling. The dispersion relation is subsequently found by computing the eigenfrequencies of the coupled meshes for a given wavenumber. The scheme was implemented in the standard finite element code ABAQUS. Dispersion relations for a 2-dimensional laminate were computed and compared with an analytical solution in order to validate the method. As an example the dispersion relation in a hexagonal fiber composite was computed and the results were compared with experiments and an existing approximate theory. Agreement was very good for waves propagating along the fibers and satisfactory for waves propagating perpendicular to the fibers. One drawback of the method is that only real valued wavenumbers can be used.

Paper 2 *Dispersion of waves in composite laminates with transverse matrix cracks, finite element and plate theory computations.* Matrix cracking in a composite laminate will affect wave propagation. This was studied using two methods. In the first approach it was assumed that the laminate is cracked periodically and the method from paper 1 was used to compute the dispersion relations. It was found that for wavelengths down to the order of laminate thickness, the cracks' influence is mainly a reduced stiffness. This inspired the second approach where a first order shear deformation laminate model was developed for laminates with matrix cracks. This model may be viewed as a two step homogenization. In the first step, the cracked plies are replaced by uncracked plies with reduced stiffnesses. The regular first order shear deformation laminate theory is then applied using the reduced ply stiffnesses. Both symmetric and unsymmetric laminates where studied and the two approaches compared favorably. The effects of crack closure was not modeled. Crack closure can have large effects on wave propagation, but in real laminates residual stresses tend to keep the cracks open, and the displacements due to wave propagation are usually small.

Paper 3 *Micromechanical modeling of transient waves from matrix cracking and fiber fracture in laminated beams.* The transient wave propagation from matrix cracking and fiber fracture in a thin laminated beam of infinite length was modeled. The method developed in paper 1 was used to compute dispersion relations and mode forms for the two lowest branches of extensional and bending (in two directions) wave propagation. Based on the mode forms, displacement fields were assumed and Hamilton's principle was used to derive a higher order beam model. The matrix cracking and fiber fracture were translated to known time dependent volume forces, which in turn were used to calculate generalized beam forces. The equations of motion, including the generalized forces, were then formally solved using Fourier transforms and mode superposition. The time response was found by an asymptotically valid inversion of the formal solution, using residue calculus and the stationary phase method. It was found that matrix cracking and fiber fracture excite several modes of propagation in a laminated beam. Matrix cracking was found to be a slow event compared to fiber fracture in the sense that the response from matrix cracking to a large extent was associated with low frequencies. The applicability of this method to acoustic emission experiments is mainly limited by two factors. Firstly, the developed beam model is valid up to frequencies corresponding to 50 kHz in a typical acoustic emission experiment, which is too low. Secondly, the inversion method used requires unrealistic distances between source and receiver - typically 50 beam widths. This could be alleviated by using the inversion method from paper 4.

Paper 4 *Numerical modeling of acoustic emission in laminated tensile test specimen.* This paper is also concerned with modeling transient wave propagation from matrix cracking and fiber fracture in a thin laminated beam, or tensile test specimen, of infinite length. In this case the cross section was discretized using finite elements, and a system of differential equations for the nodal displacements were derived using Hamilton's principle. Nodal forces from the same volume

forces as used in paper 3 (from a matrix crack and fiber fracture) were included in the differential equations. The system was formally solved using Fourier transforms and mode superposition, including attenuated modes. The formal solution was then inverted using residue calculus followed by FFT. A total of 64 nine node elements were used, and the maximum frequency used in the computations corresponds to 300 kHz in a typical acoustic emission experiment. The resulting time responses indicated that dispersion is a very important phenomenon in these kinds of experiments. It was also seen that torsional modes of wave propagation, which were not included in paper 3, give important contributions to the motion in the specimen. Finally, a method to measure average matrix crack propagation velocity was suggested.

6. REFERENCES

1. Aalami, B. (1973). Waves in prismatic guides of arbitrary cross section. *Journal of Applied Mechanics* **40**, 1067-1072.
2. Burridge, R. and Knopoff, L. (1964). Body force equivalents for seismic dislocations. *Bulletin of the Seismological Society of America* **54**(6), 1875-1888.
3. Ceranoglu, A. N. and Pao, Y.-H. (1981). Propagation of elastic pulses and acoustic emission in a plate, Parts 1-3. *Journal of Applied Mechanics* **48**, 125-147.
4. Eggers, H., Goetting, H. C. and Bäumel, H. (1994). Synergism between layer cracking and delaminations in multidirectional laminates of carbon-fibre-reinforced epoxy. *Composites Science and Technology* **50**, 343-354.
5. Eitzen, D. and Breckenridge, F. R. (1987). Acoustic Emission Sensors and their Calibration, *Nondestructive Testing Handbook (2nd ed.) Vol 5., Paul McIntire ed.*, American Society for Nondestructive Testing.
6. Graff, K. F. (1991) *Wave motion in elastic solids.* Dover Publications, Inc., New York, New York.
7. Jamison, R. D. & Reifsnider, K. L. (1982). Advanced fatigue damage development in graphite epoxy laminates. *Report AFWAL TR-82-3103*. Virginia Polytechnic Institute and State University, Blacksburg, VA.
8. Yang R. and Mal A. K. (1994). Multiple Scattering of Elastic Waves in a Fiber-Reinforced Composite. *J. Mech. Phys. Solids* **42**, 1945-1968